Modal behaviour of longitudinally perforated nanobeams

Hassina Ziou[1] and Mohamed Guenfoud[2]

[1] *National Centre for Studies and Integrated Research on Building (CNERIB), Souidania, Algiers 16097, Algeria*

[2] *University of Guelma, faculty of science and technology, Department of Civil and Hydraulic Engineering, BP 401 Guelma 24000, Algeria*

Corresponding author:
Hassina Ziou
h.ziou@cnerib.edu.dz

Received:
August 13, 2023

Accepted:
November 10, 2023

Published:
December 7, 2023

Citation:
Ziou, H.; and Guenfoud, M. (2023). Modal behaviour of longitudinally perforated nanobeams. *Advances in Civil and Architectural Engineering*. Vol. 14, Issue No. 27. pp.143-159
https://doi.org/10.13167/2023.27.10

ADVANCES IN CIVIL AND ARCHITECTURAL ENGINEERING (ISSN 2975-3848)

Faculty of Civil Engineering and Architecture Osijek
Josip Juraj Strossmayer University of Osijek
Vladimira Preloga 3
31000 Osijek
CROATIA

Abstract:
Nano-electro-mechanical systems (NEMS) require perforated beams for structural integrity. Hole sizes, hole numbers, and scale effects need to be modelled appropriately in their design. This paper presents a new finite element model to investigate the modal behaviour of longitudinally perforated nanobeams (LPNBs) using the classical Euler–Bernoulli beam theory. A symmetric array of holes arranged parallel to the length direction of the beam with equal spacing was assumed for the perforation. The non-local Eringen's differential form was used to incorporate the nanoscale sizes. The accuracy of the proposed model was verified by comparing the obtained results with the available analytical solutions for fully filled nanobeams. The effects of aspect ratios, non-local parameters, boundary conditions, and perforation characteristics on the modal behaviour of LPNBs were investigated. The non-local parameter reduced the natural frequency owing to a decrease in the stiffness of the structures. However, the perforation filling ratio led to higher values of the fundamental frequency. Furthermore, compared with other boundary conditions, clamped–clamped boundary conditions demonstrated the best performance in terms of the maximum frequency.

Keywords:
longitudinally perforated nanobeam; non-local elasticity; finite element method; Euler–Bernoulli beam theory

1 Introduction

Micro-/nano-structured devices have become a prominent focus of research in engineering and materials science owing to rapid progress in nanoscience and nanotechnology. Nanobeams are characterised by their unique structural properties and have widespread applications in various fields, such as Nano systems, nanodevices, atomic force microscopes, biosensors, nanoprobes, nanowires, nanoactuators, and nano-electro-mechanical systems (NEMS). In the framework of Eringen's non-local theory of elasticity, the stress experienced by a specific point within an elastic continuum is influenced by the surrounding strains, as opposed to classical mechanics, in which the stress is solely dependent on the strain at that point. Considering these developments, the analysis of perforated nanobeams has garnered significant attention from the scientific community owing to their diverse applications in areas, such as heat exchangers, nuclear power plants, filtration systems, and NEMS.

Abdelrahman et al. [1] performed a dynamic analysis of perforated nanobeams under the action of a moving mass using a non-local strain gradient theory. Almitani et al. [2] developed a closed-form solution to study the static bending and critical buckling of a nanobeam perforated by a square hole, including the surface energy impacts. Using an analytical approach, Abdelrahman et al. [3] examined the combined influence of the microstructure and surface energy on the bending behaviour of perforated nanobeams (PNBs). Esen et al. [4] proposed a modified continuum mathematical model based on the modified coupled stress theory to study the dynamic behaviour of Timoshenko perforated microbeams subjected to moving loads. Eltaher and Abdelrahman [5] conducted an analytical study on the bending and buckling stability of square cut-out nanobeams, considering the incorporation of nanoscale effects through surface energy properties. Eltaher and Mohamed [6] examined the effects of long-range atomic interactions, hole perforation size, and the number of hole rows on the vibration response of non-local PNBs under various boundary conditions. Abdelrahman and Eltaher [7] investigated the static deflection and stability behaviour of PNBs by considering the impact of the surface energy and different beam theories. Eltaher et al. [8, 9] employed numerical methods and the finite element technique to investigate the static deflection and natural frequencies of a piezoelectric non-local Euler–Bernoulli PNB. This study also focused on exploring the influence of nanoscale effects and surface energy on the behaviour of the beam. Abdelrahman et al. [10] introduced an integrated model and analytical approach to investigate the free and forced vibration behaviours of perforated slender/short beams. Eltaher et al. [11, 12] conducted analytical studies on the mechanical bending, buckling, and vibration responses of simply supported non-local PNBs using the modified Euler–Bernoulli and Timoshenko beam theories. Bourouina et al. [13] investigated the impact of thermal loads and size effects on the vibration characteristics of slender non-local PNBs featuring an array of square holes. A theoretical analysis of vibration, buckling, and bending of nanoplates and nanobeams has been carried out by Chakraverty and Behera [14]. Luschi and Pieri [15] derived analytical expressions for the equivalent bending stiffness of Euler–Bernoulli beams with perforations. They also utilised a previous study to calculate the resonance frequencies of perforated beams [16, 17].

The studies presented herein have significantly advanced the understanding of the behaviour of transversally PNBs characterised by cut-outs oriented in the transverse direction. These investigations provided valuable insights into the dynamic and static responses of nanobeams under various conditions. However, the absence of prior studies that specifically address the dynamic analysis of longitudinally perforated nanobeams (LPNBs) underscores the importance of further research in this domain.

This paper presents a thorough investigation of the modal behaviour of LPNBs through the development of a new finite element model. This model characterises LPNBs with a symmetric array of holes arranged parallel to the length of the beam with equal spacing. Nanoscale sizes are incorporated using the non-local Eringen's differential form. The proposed model is validated via a comparison with existing analytical solutions for fully filled nanobeams, which demonstrates excellent agreement. Furthermore, finite element numerical results are provided

in both tabular and graphical formats to examine the influence of various factors, such as the aspect ratios, non-local parameters, boundary conditions, and perforation characteristics, on the modal behaviour of the LPNBs.
The presented results serve as a valuable reference for future research on LPNBs and contribute significantly to the field.

2 Problem formulation

2.1 Geometrical adaptation

To investigate the mechanical behaviour of LPNBs efficiently, it is imperative to incorporate periodicity into their mathematical model. Figure 1 illustrates the geometric characteristics of an LPNB. The cross-sectional area of the nanobeam consists of regularly spaced square cut-outs, characterised by parameters, such as the number of hole rows per cross-section (N), perforation filling ratio (α), spatial perforation period (l_s), spatial period (t_s), and the side length of the holes (l_s-t_s). Luschi and Pieri's formula [17] provides an expression for the perforation filling ratio of perforated beams as follows:

$$\alpha = \frac{t_s}{l_s}, 0 \leq \alpha \leq 1 \tag{1}$$

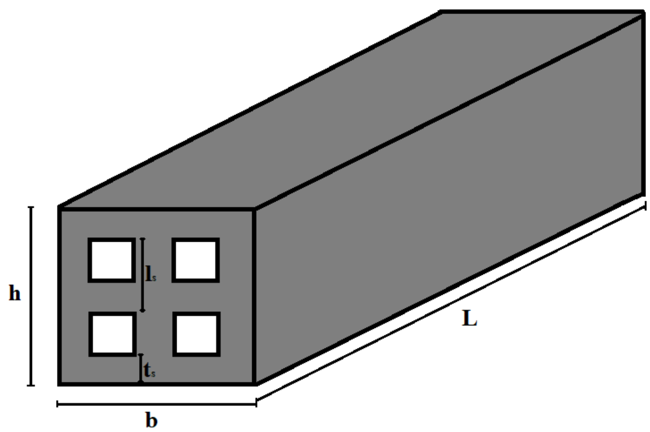

Figure 1. Geometry of a longitudinally perforated squared PNB

The perforation filling ratio of a PNB, as indicated by Eq. (1), is crucial: When the spatial period (t_s) approaches zero, and consequently, the perforation filling ratio (α) also tends to zero, it represents a scenario of a fully PNB. Conversely, as t_s approaches ls, and α approaches unity, it signifies a fully filled solid nanobeam, eliminating any perforations.

2.2 Euler–Bernoulli beam theory

The displacement field of the classical Euler–Bernoulli beam theory can be expressed as:

$$u(x,z,t) = u_0(x,t) - z\frac{\partial w_0(x,t)}{\partial x} \tag{2a}$$

$$w(x,z,t) = w_0(x,t) \tag{2b}$$

where u_0 and w_0 represent the axial and transverse displacements of any point on the mid-plane, respectively, and t denotes the time. The only non-zero strain according to the Euler–Bernoulli beam theory is defined as:

$$\varepsilon_{xx} = \frac{\partial u_0}{\partial x} - z\frac{\partial^2 w_0}{\partial x^2} = \varepsilon_{xx}^0 - z\kappa_{xx}^0 \tag{3}$$

Where ε_{xx}^0 presents the extensional strain, and κ_{xx}^0 signifies the bending strain.

2.3 Equation of motion

Hamilton's principle [18] states that:

$$\int_{t_1}^{t_2} (\delta U - \delta T)\, dt = 0 \tag{4}$$

The virtual strain energy and virtual kinetic energy are given by:

$$\begin{aligned}\delta U &= b\int\int_{\frac{-h}{2}}^{+h/2} \sigma_{xx}\, \delta\varepsilon_{xx} dz dx = b\int\int_{\frac{-h}{2}}^{+h/2} \sigma_{xx}\,(\delta\varepsilon_{xx}^0 - z\delta\kappa_{xx}^0) dz dx \\ &= b\int (N\delta\varepsilon_{xx}^0 - M\delta\kappa_{xx}^0)\, dx\end{aligned} \tag{5a}$$

$$\begin{aligned}\delta T &= b\int\int_{-h/2}^{+h/2} \rho\left[\left(\frac{\partial u_0}{\partial t} - z\frac{\partial^2 w_0}{\partial t\partial x}\right)\left(\frac{\partial \delta u_0}{\partial t} - z\frac{\partial^2 \delta w_0}{\partial t\partial x}\right) + \frac{\partial w_0}{\partial t}\frac{\partial \delta w_0}{\partial t}\right] dz dx \\ &= b\int\left[\begin{matrix} I_0\left(\frac{\partial u_0}{\partial t}\frac{\partial \delta u_0}{\partial t} + \frac{\partial w_0}{\partial t}\frac{\partial \delta w_0}{\partial t}\right) - I_1\left(\frac{\partial u_0}{\partial t}\frac{\partial^2 \delta w_0}{\partial t\partial x} + \frac{\partial^2 w_0}{\partial t\partial x}\frac{\partial \delta u_0}{\partial t}\right) + \\ I_2\frac{\partial^2 w_0}{\partial t\partial x}\frac{\partial^2 \delta w_0}{\partial t\partial x}\end{matrix}\right] dx\end{aligned} \tag{5b}$$

where b is the beam width.
The resultant force and moment are expressed as follows:

$$N = \int_{-h/2}^{+h/2} \sigma_{xx} dz \tag{6a}$$

$$M = \int_{-h/2}^{+h/2} z\sigma_{xx} dz \tag{6b}$$

The mass moment of inertia is formulated as follows:

$$\begin{Bmatrix} I_0 \\ I_1 \\ I_2 \end{Bmatrix} = \int_{-h/2}^{+h/2} \rho \begin{Bmatrix} 1 \\ z \\ z^2 \end{Bmatrix} dz \tag{6c}$$

By substituting Eq. (5) into Eq. (4), the Euler–Lagrange equation is obtained as follows:

$$\begin{aligned}\frac{\partial N}{\partial x} &= I_0\frac{\partial^2 u_0}{\partial t^2} - I_1\frac{\partial^3 w_0}{\partial x\partial t^2} \\ \frac{\partial^2 M}{\partial x^2} &= I_0\frac{\partial^2 w_0}{\partial t^2} + I_1\frac{\partial^3 u_0}{\partial x\partial t^2} - I_2\frac{\partial^4 w_0}{\partial x^2\partial t^2}\end{aligned} \tag{7}$$

2.4 Non-local continuum beam model

In the classical elasticity theory, the stress at a point depends only on the strain at that point. In contrast, the non-local elasticity theory asserts that stress at a point is influenced by strains across the entire continuum.
The formula for the non-local stress tensor at a particular point 'x' can be found in reference [19].

$$\sigma = \int_V K(|x' - x|, \tau)\, T(x')\, dx' \quad (8a)$$

$$T(x) = C(x) : \varepsilon(x) \quad (8b)$$

Where T(x) is the classic macroscopic stress tensor at point x, ε(x) is the strain tensor, C(x) is the fourth-order elasticity tensor and denotes the 'double-dot product', K(|x' − x|, τ) is the non-local modulus or attenuation function incorporating into the constitutive equations the non-local effects at the reference point x produced by the local strain at the source x', |x' – x| is the Euclidean distance, $\tau = e_0 a/l$ is defined as a small scale factor, where e_0 is a constant to adjust the model to match the reliable results obtained by experiments or other models, a is the internal characteristic length (e.g. lattice parameter, C–C bond length, granular distance, crack length, wavelength), and l is the external length.

In a beam structure, the shortness and width are significantly smaller than the length. Therefore, the integral constitutive relations can be represented in an equivalent differential form as:

$$(1 - \tau^2 l^2 \nabla^2)\sigma = t \quad (9)$$

For a non-local Euler–Bernoulli beam, Eq. (9) can be written as:

$$\sigma_{xx} - \mu \frac{\partial^2 \sigma_{xx}}{\partial x^2} = E\varepsilon_{xx},\ \mu = a^2 e_0^2 \quad (10)$$

By integrating Eq. (10) across the cross-sectional area of the beam, the axial force–strain relationship is obtained as follows:

$$N - \mu \frac{\partial^2 N}{\partial x^2} = EA\varepsilon_{xx}^0 \quad (11a)$$

By multiplying Eq. (10) by 'z' and integrating it across the cross-sectional area, the moment–curvature relation is obtained as follows:

$$M - \mu \frac{\partial^2 M}{\partial x^2} = EI\kappa_{xx}^0 \quad (11b)$$

Differentiating Eq. (7a) once with respect to 'x' and substituting the outcome into Eq. (10-a) yields:

$$N = EA\frac{\partial u_0}{\partial x} + \mu\left[I_0 \frac{\partial^3 u_0}{\partial x \partial t^2} - I_1 \frac{\partial^4 w_0}{\partial x^2 \partial t^2}\right] \quad (12a)$$

By substituting the second derivative of M from Eq. (7-b) into Eq. (10-b), the moment can be obtained as follows:

$$M = EI\frac{\partial^2 w_0}{\partial x^2} + \mu\left[I_0 \frac{\partial^2 w_0}{\partial t^2} + I_1 \frac{\partial^3 u_0}{\partial x \partial t^2} - I_2 \frac{\partial^4 w_0}{\partial x^2 \partial t^2}\right] \quad (12b)$$

3 Numerical formulation

Based on Hamilton's principle, the substitution of Eq. (12) into Eq. (5), and the substitution of the resulting expression into Eq. (4), the following deduced variational statement for the non-local Euler–Bernoulli beam is obtained:

$$\int_0^t \int_0^L \left\{ \begin{array}{l} \left(-EA\frac{\partial u_0}{\partial x}\frac{\partial \delta u_0}{\partial x} + EI\frac{\partial^2 w_0}{\partial x^2}\frac{\partial^2 \delta w_0}{\partial x^2} \right) + \left(I_0\frac{\partial u_0}{\partial t}\frac{\partial \delta u_0}{\partial t} - \mu I_0\frac{\partial^3 u_0}{\partial t^2 \partial x}\frac{\partial \delta u_0}{\partial x} \right) + \\ \left(I_0\frac{\partial w_0}{\partial t}\frac{\partial \delta w_0}{\partial t} + \mu I_0\frac{\partial^2 w_0}{\partial t^2}\frac{\partial^2 \delta w_0}{\partial x^2} + I_2\frac{\partial^2 w_0}{\partial t \partial x}\frac{\partial^2 \delta w_0}{\partial t \partial x} - \mu I_2\frac{\partial^4 w_0}{\partial t^2 \partial x^2}\frac{\partial^2 w_0}{\partial x^2} \right) + \\ \left(I_1\frac{\partial^2 w_0}{\partial t \partial x}\frac{\partial \delta u_0}{\partial t} + \mu I_1\frac{\partial^3 u_0}{\partial t^2 \partial x}\frac{\partial^2 \delta w_0}{\partial x^2} - I_1\frac{\partial \delta u_0}{\partial t}\frac{\partial^2 \delta w_0}{\partial t \partial x} + \mu I_1\frac{\partial^4 w_0}{\partial t^2 \partial x^2}\frac{\partial^2 \delta u_0}{\partial x} \right) \end{array} \right\} dxdt \quad (13)$$

3.1 Numerical results and discussion

This section is divided into two sub-sections: The first is devoted mainly to comparing the proposed model with those previously published for fully filled nanobeams. The second sub-section focuses on an analysis of LPNBs.

3.1.1 *Model validation*

This section is primarily dedicated to the verification of the proposed model via a comparison with previously published models. The finite element system of equations can be succinctly represented as:

$$[K]\{U\} = \omega^2[M]\{U\} \quad (14)$$

where {U} represents the degree of freedom vector, [M] and [K] denote the mass and stiffness matrices, respectively, and ω denotes the circular frequency. The geometrical and material properties of the non-local beam used in this section adhere to those established by Behera and Chakraverty [14].

To assess the validity of the proposed methodology, the dimensionless fundamental frequency $\left(\lambda = \omega L^2 \sqrt{\frac{\rho A}{EI}}\right)$ was obtained and compared with the results obtained by Behera and Chakraverty [14] for various non-local parameters and different boundary conditions for fully filled nanobeams (Table 1). The comparison presented in Table 1 demonstrates a favourable agreement between the predicted values obtained using the current method and the corresponding values reported by Behera and Chakraverty [14] using the dynamic quadrature method.

Table 1. Comparison of the dimensionless fundamental frequency $\sqrt{\lambda}$ of a fully filled Euler–Bernoulli nanobeam (L = 10 m, E = 30 MPa, ρ = 1, h = 0,1, ν = 0,3)

Methodology	BCs	Non-local parameter					
		$\mu = 0$	$\mu = 1$	$\mu = 2$	$\mu = 3$	$\mu = 4$	$\mu = 5$
Chakraverty, S. and Behera, L. [14]	S–S	3,1416 3,1416	3,0738 3,0685	3,0128 3,0032	2,9574 2,9444	2,9574 2,8908	2,8601 2,8418
	C–C	4,7423 4,7300	4,6008 4,5945	4,4776 4,4758	4,3690 4,3707	4,2722 4,2766	4,1850 4,1917
	C–S	3,9361 3,9266	3,8274 3,8209	3,7321 3,7278	3,6473 3,6448	3,5712 3,5701	3,5023 3,5024
	C–F	1,8769 1,8751	1,8555 1,8792	1,8352 1,8833	1,8158 1,8876	1,7973 1,8919	1,7797 1,8964

3.1.2 *Parametric study*

After the validation of the fully filled nanobeam, the modal behaviour of the LPNBs for various end-boundary conditions, aspect ratios, non-local parameters, and perforation filling ratios is studied.

The material properties are defined as follows: Young's modulus (E) = 30 MPa, Poisson's ratio (ν) = 0,3; density (ρ) = 1, and beam dimensions (b = h = 0,1).

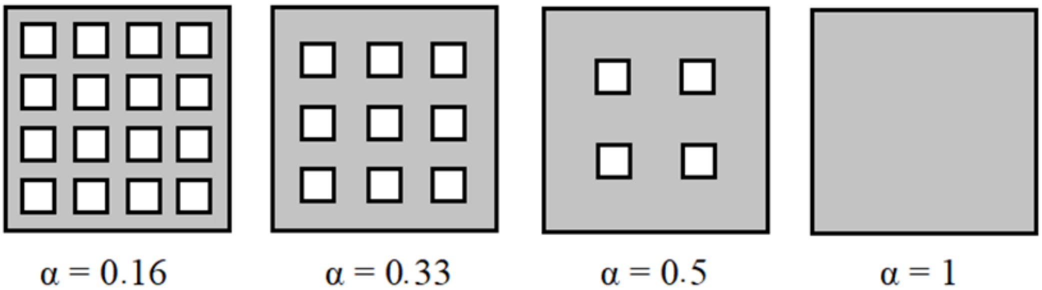

Figure 2. Beam geometry details with various opening positions

The variation of the first three dimensionless frequency parameters is presented, considering various aspect ratios (L/h = 10, 20, 100), non-local parameters (μ = 0, 1, 2, 3, 4, and 5), and perforation filling ratios (α = 0,16; 0,33; 0,5, and 1 (see Figure 2)) of the PNB as shown in Tables 2-7. For a constant perforation filling ratio and aspect ratio, an increase in the non-local parameter leads to a decrease in the first three frequencies, because introducing the non-locality effect leads to a softening effect, resulting in smaller values of the fundamental frequency parameters. Note that the short nanobeam (L/h = 10) is more affected by the non-local parameters than the slender nanobeams (L/h = 20, 100). Furthermore, the influence of the perforation filling ratio on the fundamental frequency parameter is more prominent for the short nanobeam (L/h = 10) than for the slender nanobeams (L/h = 20, 100). Nevertheless, the Euler–Bernoulli model tends to underestimate the third mode for the short nanobeam (L/h = 10).

Table 2. Variation of the first three dimensionless frequency parameters (λ_1, λ_2, and λ_3) for different slenderness ratios (L/h) and perforation filling ratios (α) for a simply supported nanobeam (μ = 0)

L/h	λ_i	α = 0,16	α = 0,33	α = 0,50	α = 1,00
10	i = 1	9,9814	9,9225	9,9138	9,9105
	i = 2	33,1086	40,3501	40,2545	40,1489
	i = 3	41,3679	47,9234	50,1843	54,4810
20	i = 1	9,8972	9,8827	9,8816	9,8798
	i = 2	39,9259	39,6902	39,6714	39,6418
	i = 3	66,1660	89,9568	89,8573	89,7022
100	i = 1	9,8707	9,8701	9,8701	9,8700
	i = 2	39,4963	39,4871	39,4864	39,4852
	i = 3	88,9533	88,8827	88,8768	88,8681

Table 3. Variation of the first three dimensionless frequency parameters (λ_1, λ_2, and λ_3) for different slenderness ratios (L/h) and perforation filling ratios (α) for a simply supported nanobeam (μ = 1)

L/h	λ_i	α = 0,16	α = 0,33	α = 0,50	α = 1,00
10	i = 1	9,5031	9,4573	9,4497	9,4479
	i = 2	32,7074	33,7438	33,7021	33,6723
	i = 3	34,1105	47,3417	49,5752	53,8201
20	i = 1	9,7759	9,7624	9,7613	9,4238
	i = 2	38,0130	37,8293	37,8147	33,4898
	i = 3	65,9629	81,0798	81,0232	64,9419
100	i = 1	9,8658	9,8653	9,8652	9,4162
	i = 2	39,4185	39,4093	39,4086	33,4309
	i = 3	88,5608	88,4899	88,4841	64,7265

Table 4. Variation of the first three dimensionless frequency parameters (λ_1, λ_2, and λ_3) for different slenderness ratios (L/h) and perforation filling ratios (α) for a simply supported nanobeam (μ = 2)

L/h	λ_i	α = 0,16	α = 0,33	α = 0,50	α = 1,00
10	i = 1	9,0876	9,0518	9,0453	9,0445
	i = 2	29,6704	29,5884	29,5698	29,5716
	i = 3	32,3191	46,7834	48,9920	53,0244
20	i = 1	9,6591	9,6464	9,6453	9,0257
	i = 2	36,3514	36,2081	36,1967	29,5256
	i = 3	65,7620	74,4327	74,4006	53,2074
100	i = 1	9,8610	9,8604	9,8604	9,0197
	i = 2	39,3411	39,3320	39,3313	29,5139
	i = 3	88,1734	88,1023	88,0966	53,4363

Table 5. Variation of the first three dimensionless frequency parameters (λ_1, λ_2, and λ_3) for different slenderness ratios (L/h) and perforation filling ratios (α) for a simply supported nanobeam (μ = 3)

L/h	λ_i	α = 0,16	α = 0,33	α = 0,50	α = 1,00
10	i = 1	8,7222	8,6944	8,6887	8,6887
	i = 2	26,6153	26,6668	26,6603	26,6776
	i = 3	31,9455	45,7909	45,8482	45,9714
20	i = 1	9,5464	9,5344	9,5334	8,6741
	i = 2	34,8906	34,7792	34,7703	26,7025
	i = 3	65,5637	69,2088	69,1920	46,2448
100	i = 1	9,8561	9,8556	9,8555	8,6695
	i = 2	39,2641	39,2551	39,2544	26,7113
	i = 3	87,7911	87,7197	87,7141	46,3990

Table 6. Variation of the first three dimensionless frequency parameters (λ_1, λ_2, and λ_3) for different slenderness ratios (L/h) and perforation filling ratios (α) for a simply supported nanobeam (μ = 4)

L/h	λ_i	α = 0,16	α = 0,33	α = 0,50	α = 1,00
10	i = 1	8,3976	8,3763	8,3712	8,3719
	i = 2	24,3439	24,4689	24,4692	24,4950
	i = 3	31,5856	40,9609	41,0163	41,1441
20	i = 1	9,4375	9,4262	9,4253	8,3606
	i = 2	33,5932	33,5075	33,5006	24,5599
	i = 3	65,0553	64,9596	64,9527	41,4439
100	i = 1	9,8513	9,8507	9,8507	8,3571
	i = 2	39,1876	39,1787	39,1780	24,5816
	i = 3	87,4136	87,3422	87,3367	41,6277

Table 7. Variation of the first three dimensionless frequency parameters (λ_1, λ_2, and λ_3) for different slenderness ratios (L/h) and perforation filling ratios (α) for a simply supported nanobeam (μ = 5)

L/h	λ_i	α = 0,16	α = 0,33	α = 0,5	α = 1
10	i = 1	8,1068	8,0907	8,0861	8,0874
	i = 2	22,5683	22,7380	22,7426	22,7732
	i = 3	31,2348	37,3897	37,4459	37,5683
20	i = 1	9,3322	9,3216	9,3207	8,0789
	i = 2	32,4272	32,3660	32,3608	22,8621
	i = 3	61,0984	61,4131	61,4131	37,8798
100	i = 1	9,8464	9,8459	9,8458	8,0762
	i = 2	39,1115	39,1027	39,1020	22,8915
	i = 3	87,0410	86,9694	86,9641	38,0788

Figures 3-5 present a comprehensive analysis of the impact of the perforation filling ratio and non-local parameter on the first three dimensionless frequency parameters of the nanobeams. The study considers various beam aspect ratios under simply supported boundary conditions. The figures provide valuable insights into how these factors influence the vibrational characteristics of the nanobeams, clarifying their mechanical behaviour and performance. Based on the findings in Figure 3, it can be deduced that the first frequency exhibits a slight decrease within the perforation filling ratio range of 0,16 to 0,33, whereas it decreases less significantly within the perforation filling ratio range of 0,33 to 1,00. Additionally, the first frequency experiences a gradual decrease at a low rate, as the non-locality parameter increases from 0 to 5. On the other hand, the second frequency shows a substantial increase within the perforation filling ratio range of 0,16 to 0,33, compared with that within the range of 0,33 to 1,00. Furthermore, the effect of non-locality on the second frequency diminishes as the non-locality parameter increases. In addition, the influence of the non-locality parameter on the third frequency is relatively weaker compared with that on the first and second frequencies. However, the perforation filling ratio remains effective across the entire range of 0,16 to 1,00 while maintaining a constant non-local parameter.

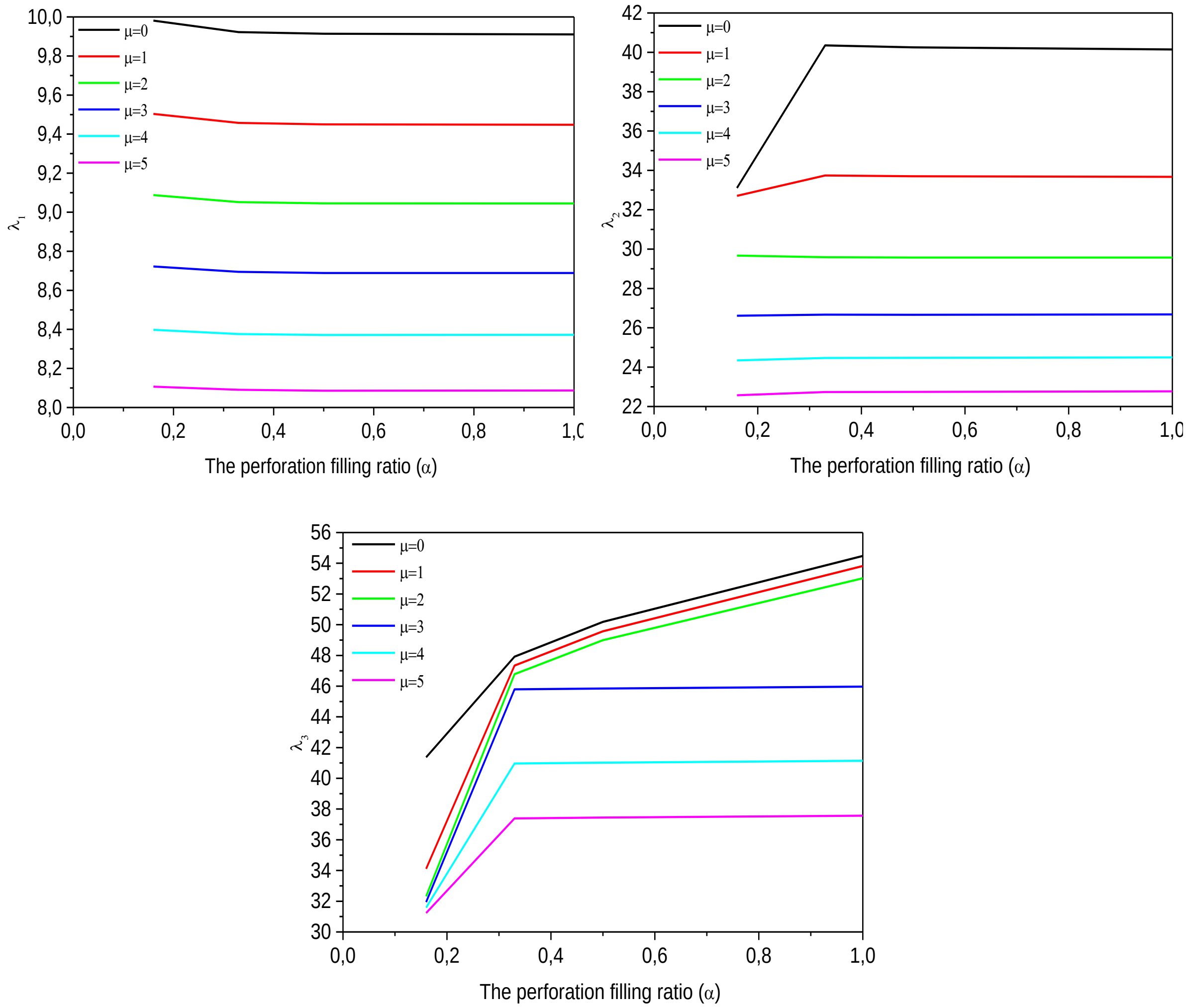

Figure 3. Effect of the perforation filling ratio and non-local parameter on the first three dimensionless frequency parameters for a simply supported nanobeam (L/h = 10)

The data in Figure 4 reveal that the first two frequencies remain constant in the perforation filling ratio range of 0,16 to 0,50. However, noticeable effects of the perforation filling ratio are observed only in the higher range of 0,5 to 1,0. In contrast, the third frequency shows a notable increase for the perforation filling ratio range of 0,16 to 0,33, but experiences a significant decrease in the range of 0,5 to 1,0. This demonstrates the high sensitivity of the third frequency to changes in the perforation filling ratio.

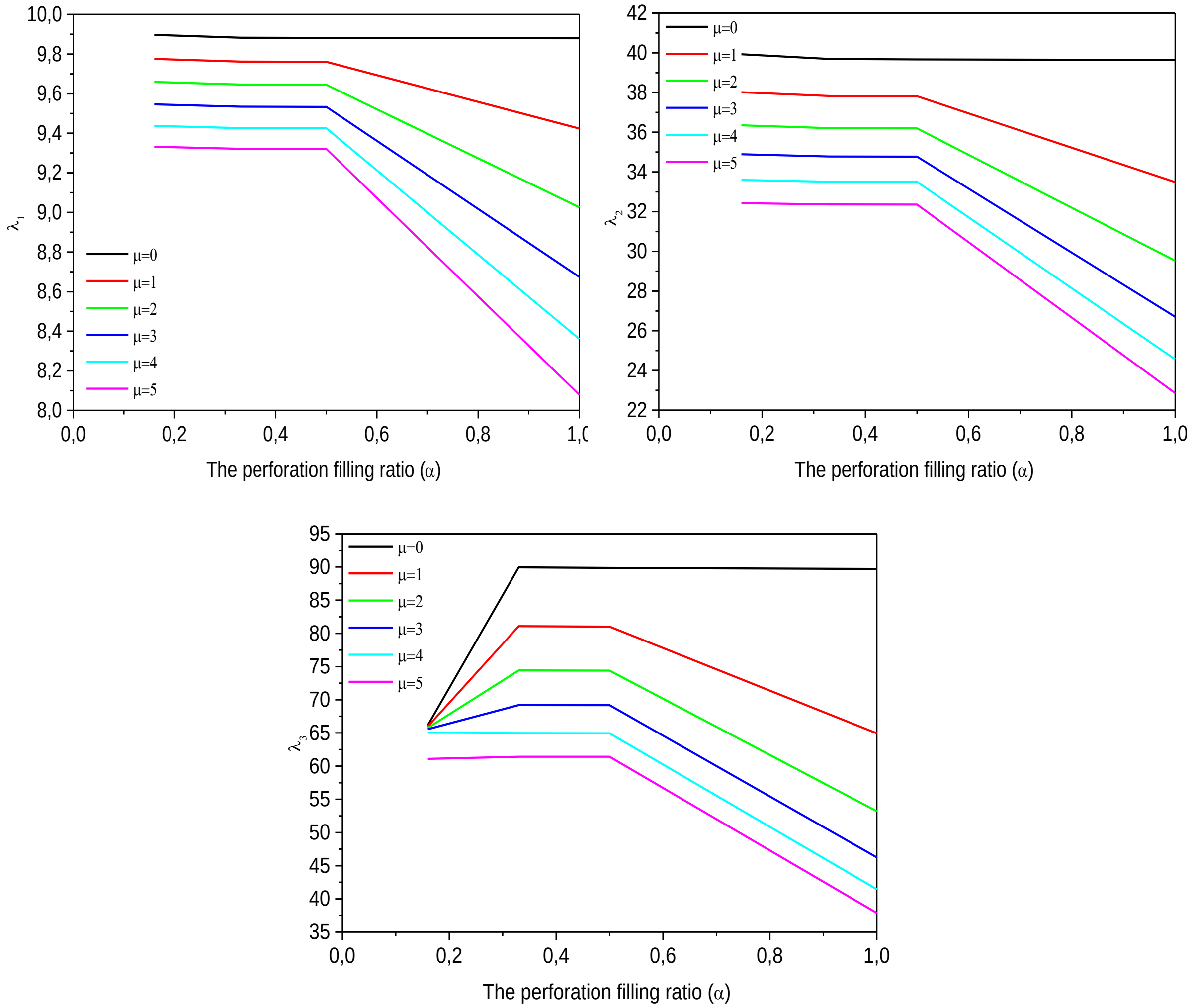

Figure 4. Effect of the perforation filling ratio and non-local parameter on the first three dimensionless frequency parameters for a simply supported nanobeam (L/h = 20)

Figure 5 illustrates the variation in the first three fundamental frequencies with changes in the non-locality parameter and perforation filling ratio at L/h = 100. For μ = 0, there is no significant variation in the frequencies with respect to the change in the perforation filling ratio. For all other values of the non-local parameter, the frequencies demonstrate a notable and abrupt decrease when the perforation filling ratio is within the range of 0,5 to 1,0.
Tables 8-10 provide insights into the influence of the non-local parameter and perforation filling ratio on the first three dimensionless frequencies for the clamped–clamped (C–C), clamped–simply supported (C–S), and clamped–free (C–F) short nanobeams. Increasing the filling ratio results in a decrease in the fundamental frequency. Similarly, with an increase in the non-local parameter, the frequencies also decrease. Notably, the effects of the perforation filling ratio on the second and third frequencies differ, indicating a high sensitivity of higher frequencies to changes in the perforation filling ratio.

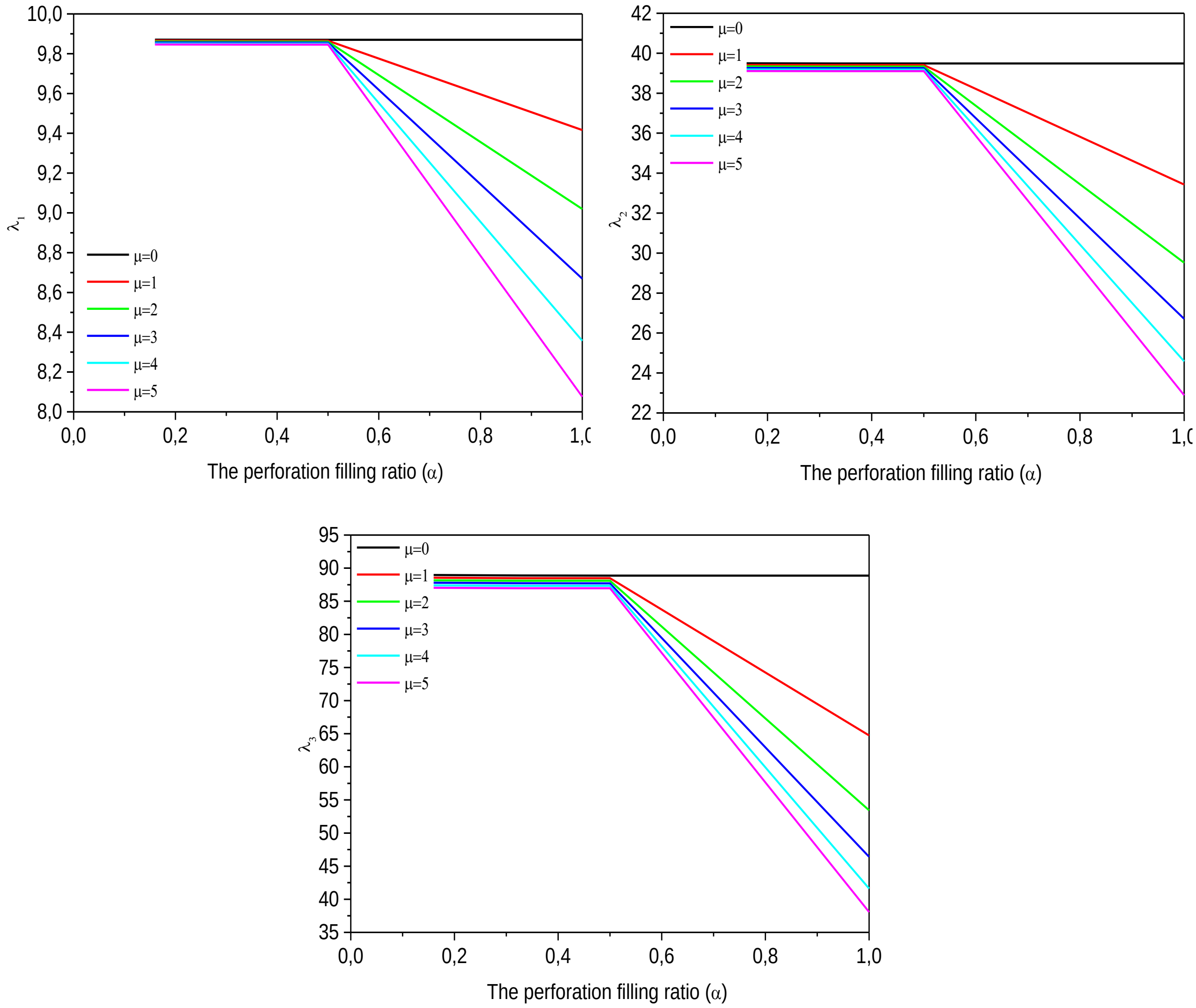

Figure 5. Effect of the perforation filling ratio and non-local parameter on the first three dimensionless frequency parameters for a simply supported nanobeam (L/h = 100)

Table 8. Variation of the first three dimensionless frequency parameters (λ_1, λ_2, and λ_3) for different slenderness ratios (L/h) and perforation filling ratios (α) for a clamped–clamped nanobeam

μ	λ_i	α = 0,16	α = 0,33	α = 0,50	α = 1,00
0	i = 1	22,6909	22,5237	22,5012	22,4896
	i = 2	65,1587	63,2761	63,1047	62,9065
	i = 3	66,4214	96,1479	100,684	109,3086
1	i = 1	21,2674	21,1846	21,1694	21,1676
	i = 2	51,3324	51,1589	51,1238	51,1222
	i = 3	63,3482	84,9962	85,0393	85,1969
2	i = 1	20,0772	20,0544	20,0444	20,0497
	i = 2	43,6651	44,0542	44,0674	44,1334
	i = 3	60,7050	68,1568	68,3081	68,6179
3	i = 1	19,0635	19,0845	19,0785	19,0888
	i = 2	38,6358	39,2508	39,2861	39,3816
	i = 3	55,8437	58,3200	58,5126	58,8748
4	i = 1	18,1872	18,2408	18,2378	18,2519
	i = 2	35,0159	35,7366	35,7826	35,8912
	i = 3	49,4578	51,9339	52,1310	52,4956

5	i = 1	17,4200	17,4984	17,4978	17,5148
	i = 2	32,2514	33,0211	33,0726	33,1873
	i = 3	44,8746	47,2902	47,4859	47,8448

Table 9. Variation of the first three dimensionless frequency parameters (λ_1, λ_2, and λ_3) for different slenderness ratios (L/h) and perforation filling ratios (α) for a clamped–simply supported nanobeam

μ	λ_i	α = 0,16	α = 0,33	α = 0,50	α = 1,00
0	i = 1	15,6225	15,5149	15,5000	15,4929
	i = 2	33,1085	47,9233	50,1842	50,8912
	i = 3	52,5824	51,1690	51,0388	54,4808
1	i = 1	14,7368	14,6645	14,6528	14,6497
	i = 2	32,7067	42,0875	42,0449	42,0224
	i = 3	42,4215	47,3416	49,5750	53,8196
2	i = 1	13,9842	13,9381	13,9287	13,9286
	i = 2	32,3191	36,5886	36,5804	36,6055
	i = 3	36,5075	46,7807	48,9878	53,1823
3	i = 1	13,3347	13,3084	13,3009	13,3030
	i = 2	31,9450	32,8083	32,8168	32,8637
	i = 3	32,5449	46,2401	48,4220	52,2719
4	i = 1	12,7669	12,7560	12,7499	12,7537
	i = 2	29,6495	30,0058	30,0232	30,0812
	i = 3	31,5838	45,7198	46,4440	46,6897
5	i = 1	12,2653	12,2663	12,2615	12,2666
	i = 2	27,4102	27,8213	27,8439	27,9078
	i = 3	31,2341	42,2239	42,3511	42,5947

Table 10. Variation of the first three dimensionless frequency parameters (λ_1, λ_2, and λ_3) for different slenderness ratios (L/h) and perforation filling ratios (α) for a clamped–free nanobeam

μ	λ_i	α = 0,16	α = 0,33	α = 0,50	α = 1,00
0	i = 1	3,5346	3,5248	3,5226	3,5228
	i = 2	22,8855	22,4296	22,3847	22,3386
	i = 3	33,1086	47,9299	50,1942	54,5003
1	i = 1	3,4538	3,4449	3,4428	3,4431
	i = 2	19,6056	19,3563	19,3287	19,3060
	i = 3	32,7238	47,0785	47,0029	46,9337
2	i = 1	3,3677	3,3697	3,3677	3,3680
	i = 2	17,2610	17,2794	17,2610	17,2502
	i = 3	39,1071	39,1279	39,1071	39,1184
3	i = 1	3,3064	3,2989	3,2969	3,2973
	i = 2	15,8537	15,7708	15,7578	15,7539
	i = 3	31,9856	34,3464	34,3488	34,3906
4	i = 1	3,2389	3,2320	3,2302	3,2306
	i = 2	14,6616	14,6165	14,6070	14,6073
	i = 3	30,6439	31,0501	31,0637	31,1191
5	i = 1	3,1751	3,1688	3,1671	3,1675
	i = 2	13,7187	13,6987	13,6915	13,6945
	i = 3	28,1310	28,5895	28,6091	28,6710

Figure 6 shows a comprehensive examination of the influence of the perforation filling ratio and non-local parameter on the fundamental frequency of a short nanobeam (L/h = 10) under various boundary conditions. Notably, the highest fundamental frequency is observed when the non-local parameter μ is set to 0. As the non-local parameter increases, the fundamental frequencies decrease for all end-boundary conditions, underscoring the significant role played by the non-local parameter in softening the fundamental frequency. Additionally, the maximum fundamental frequency is attained at a perforation filling ratio of α = 0,16, which can be attributed to a more rapid decrease in the equivalent mass of the system at this specific ratio. Moreover, the boundary conditions have a noticeable impact on the flexibility and frequency of the nanobeam. Specifically, the C–F end condition results in a more flexible nanobeam with lower frequency values, whereas the C–C end condition exhibits higher frequencies compared with the other boundary conditions. These findings indicate that both the mass and stiffness characteristics of the system play pivotal roles in determining the frequencies of the short nanobeams under consideration.

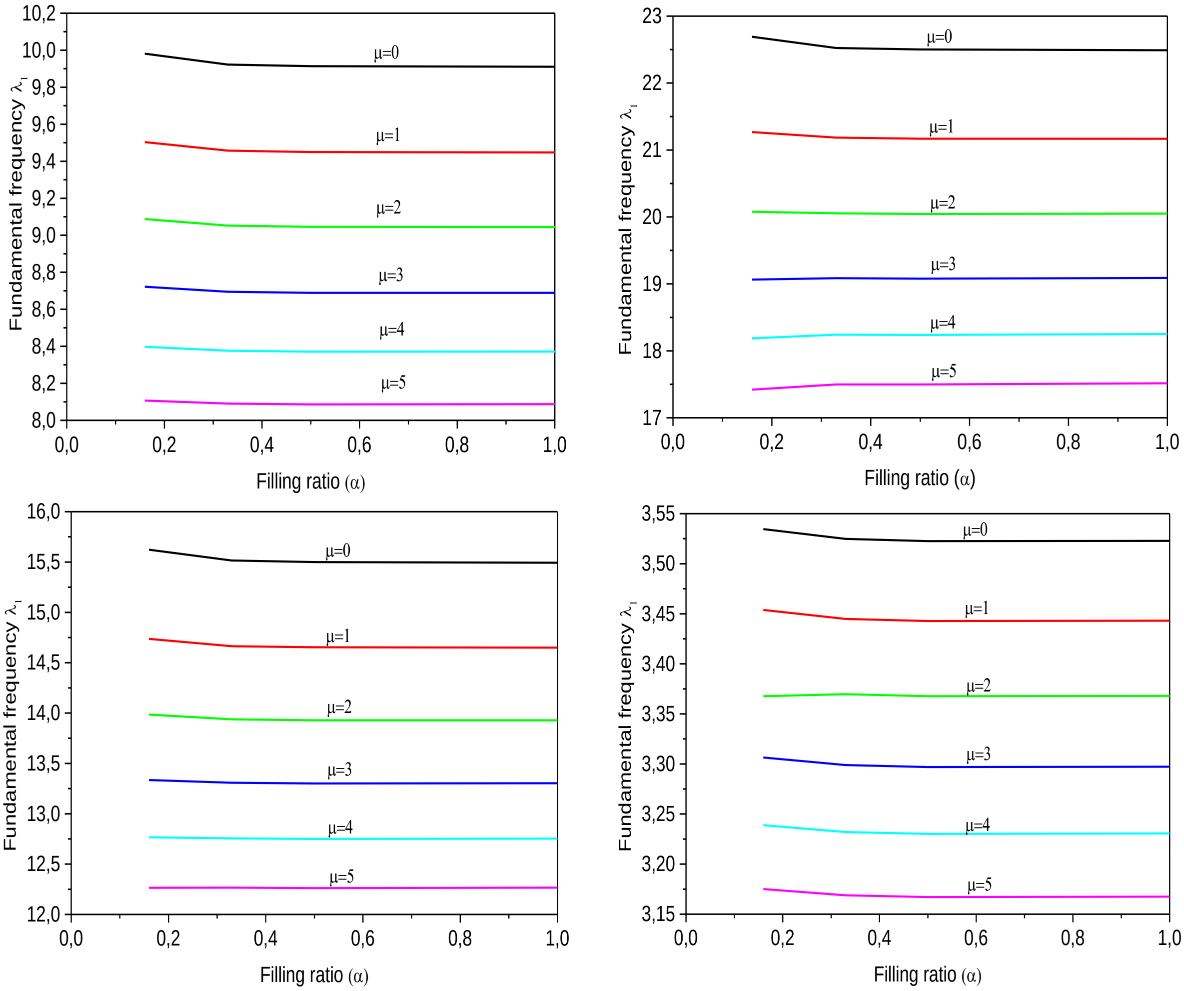

Figure 6. Variation of the fundamental frequency λ1 with the perforation filling ratio and non-local parameter of the short nanobeam (L/h = 10) for different boundary conditions (S–S; C–C; C–S; C–F)

The impacts of the non-local parameter and perforation filling ratio on the first three dimensionless frequencies of the clamped–clamped (C–C), clamped–simply supported (C–S), and clamped–free (C–F) slender nanobeams are presented in Tables 11-13 and Figure 7. As the perforation filling ratio increases, the fundamental frequency decreases slightly. Similarly, as the non-local parameter increases, the frequencies decrease slightly. These observations indicate that the influences of both the perforation filling ratio and non-local parameter on the fundamental frequency of the slender nanobeams are practically negligible. Moreover, the boundary conditions have a noticeable impact on the flexibility and frequency values of the nanobeam. The C–F end condition results in a flexible nanobeam with lower frequency values, whereas the C–C end condition displays higher frequencies compared with the other boundary conditions. For the S–S end condition, at μ = 0, there is no significant variation in the fundamental frequency with respect to the change in the perforation filling ratio. For all other values of the non-local parameter, the frequency demonstrates a notable and abrupt decrease when the perforation filling ratio is within the range of 0,5 to 1,0.

Table 11. Variation of the first three dimensionless frequency parameters (λ_1, λ_2, and λ_3) for different slenderness ratios (L/h) and perforation filling ratios (α) for a clamped–clamped nanobeam

μ	λ_i	α = 0,16	α = 0,33	α = 0,50	α = 1,00
0	i = 1	22,3764	22,3748	22,3747	22,3745
	i = 2	61,7059	61,6891	61,6878	61,6857
	i = 3	121,0466	120,9759	120,9702	120,9613
1	i = 1	22,3627	22,3611	22,3609	22,3607
	i = 2	61,5639	61,5474	61,5461	61,5440
	i = 3	120,4491	120,3805	120,3749	120,3663
2	i = 1	22,3489	22,3473	22,3472	22,3470
	i = 2	61,4228	61,4066	61,4053	61,4032
	i = 3	119,8603	119,7937	119,7883	119,7799
3	i = 1	22,3352	22,3336	22,3335	22,3333
	i = 2	61,2827	61,2667	61,2654	61,2634
	i = 3	119,2800	119,2153	119,2101	119,2020
4	i = 1	22,3215	22,3199	22,3198	22,3196
	i = 2	61,1436	61,1278	61,1265	61,1245
	i = 3	118,7080	118,6452	118,6402	118,6323
5	i = 1	22,3078	22,3059	22,3061	22,3059
	i = 2	61,0053	60,9865	60,9885	60,9865
	i = 3	118,1441	118,0706	118,0783	118,0706

Table 12. Variation of the first three dimensionless frequency parameters (λ_1, λ_2, and λ_3) for different slenderness ratios (L/h) and perforation filling ratios (α) for a clamped–simply supported nanobeam

μ	λ_i	α = 0,16	α = 0,33	α = 0,50	α = 1,00
0	i =1	15,4202	15,4192	15,4191	15,4190
	i =2	49,9896	49,9769	49,9759	49,9743
	i =3	104,3750	104,3067	104,3018	104,2943
1	i = 1	15,4113	15,4103	15,4102	15,4101
	i = 2	49,8825	49,8700	49,8690	49,8674
	i = 3	103,8853	103,8187	103,8139	103,8066
2	i = 1	15,4025	15,4014	15,4014	15,4012
	i = 2	49,7760	49,7637	49,7627	49,7611
	i = 3	103,4025	103,3375	103,3328	103,3257
3	i = 1	15,3936	15,3926	15,3925	15,3924
	i = 2	49,6703	49,6581	49,6571	49,6556
	i = 3	102,9262	102,8629	102,8583	102,8514
4	i = 1	15,3848	15,3838	15,3837	15,3836
	i = 2	49,5652	49,5531	49,5522	49,5507
	i = 3	102,4565	102,3947	102,3903	102,3835
5	i = 1	15,3760	15,3750	15,3749	15,3748
	i = 2	49,4608	49,4489	49,4479	49,4464
	i = 3	101,9932	101,9330	101,9287	101,9221

Table 13. Variation of the first three dimensionless frequency parameters (λ_1, λ_2, and λ_3) for different slenderness ratios (L/h) and perforation filling ratios (α) for a clamped–free nanobeam

µ	λ_i	α = 0,16	α = 0,33	α = 0,50	α = 1,00
0	i = 1	3,5162	3,5161	3,5161	3,5161
	i = 2	22,0426	22,0384	22,0380	22,0375
	i = 3	61,7534	61,7252	61,7229	61,7194
1	i = 1	3,5154	3,5153	3,5153	3,5153
	i = 2	22,0069	22,0027	22,0024	22,0019
	i = 3	61,5155	61,4878	61,4855	61,4820
2	i = 1	3,5146	3,5145	3,5145	3,5145
	i = 2	21,9714	21,9672	21,9669	21,9664
	i = 3	61,2803	61,2530	61,2509	61,2474
3	i = 1	3,5138	3,5137	3,5136	3,5136
	i = 2	21,9360	21,9319	21,9316	21,9311
	i = 3	61,0478	61,0210	61,0188	61,0155
4	i = 1	3,5129	3,5128	3,5128	3,5128
	i = 2	21,9009	21,8967	21,8964	21,8959
	i = 3	60,8179	60,7915	60,7894	60,7861
5	i = 1	3,5121	3,5120	3,5120	3,5120
	i = 2	21,8658	21,8617	21,8614	21,8609
	i = 3	60,5906	60,5647	60,5626	60,5593

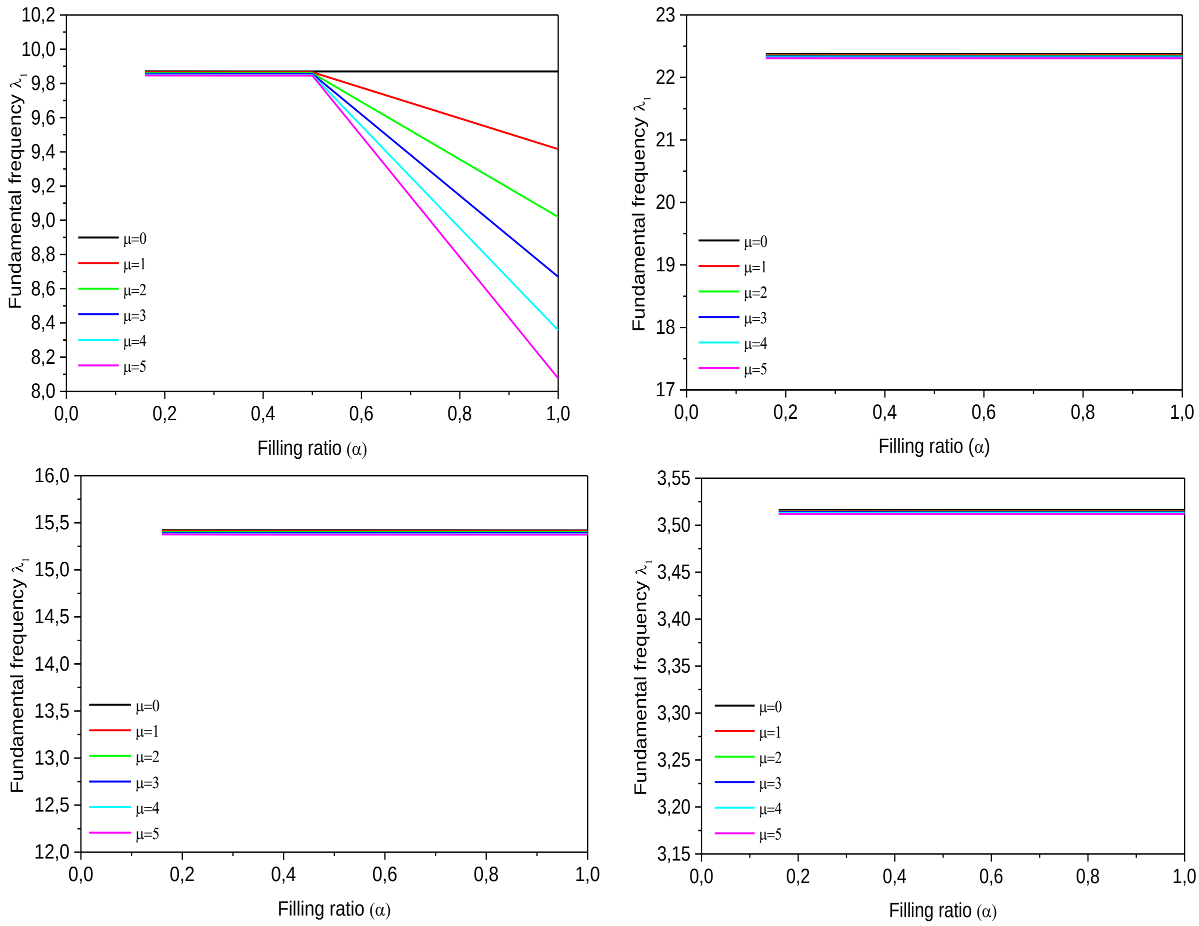

Figure 7. Variation of the fundamental frequency λ1 with the perforation filling ratio and non-local parameter of slender nanobeams (L/h = 100) for different boundary conditions (S–S; C–C; C–S; C–F)

4 Conclusions

This study conducted a comprehensive investigation of the modal behaviour of LPNBs by developing a new finite element model. This model characterises LPNBs with a symmetric array of holes arranged parallel to the length of the beam with equal spacing. A non-local Eringen differential model was applied to address the nanoscale dimensions. This paper presented novel numerical solutions and explicit formulas that have not been previously reported, which significantly contribute to the understanding of the modal behaviour of LPNBs. The study also examined the effects of the aspect ratios, non-local parameters, boundary conditions, and perforation characteristics on the modal behaviour of LPNBs.
Based on the above study, the following conclusions can be drawn:

- For a constant perforation filling ratio and aspect ratio, an increase in the non-local parameter leads to a decrease in the first three frequencies because introducing the non-locality effect leads to a softening effect, resulting in smaller values of the fundamental frequency parameters.
- The short nanobeam (L/h = 10) is more affected by the non-local parameters than the slender nanobeams (L/h = 20, 100).
- The influence of the perforation filling ratio on the fundamental frequency parameter is more prominent for the short nanobeam (L/h = 10) than for the slender nanobeams (L/h = 20, 100).
- The influences of both the perforation filling ratio and non-local parameter on the fundamental frequency of the slender nanobeams (L/h = 20, 100) are practically negligible.
- The maximum fundamental frequency is attained at a perforation filling ratio of $\alpha = 0{,}16$; which can be attributed to a more rapid decrease in the equivalent mass of the system at this specific ratio.
- Moreover, the boundary conditions have a noticeable impact on the flexibility and frequency of the nanobeam. Specifically, the C–C end condition exhibits higher frequencies compared with the other boundary conditions, whereas the C–F end condition results in a more flexible nanobeam with lower frequency values. Hence, both the mass and stiffness characteristics of the system play pivotal roles in determining the frequencies of the nanobeams under consideration.

In the design of NEMS, an appropriate selection of the perforation filling ratio, hole numbers, boundary conditions, aspect ratio, and non-local parameter enables the tailoring of the geometrical characteristics to achieve the desired goal of minimising frequencies in a perforated-beam-type structure.
Overall, this study provides valuable insights into the modal behaviours of LPNBs and offers guidance for optimising their design and performance in various applications.

Acknowledgements

The work reported in this paper was developed as a part of the authors' doctoral thesis. The authors express sincere gratitude to the reviewers for their helpful comments and suggestions.

References

[1] Abdelrahman, A. A.; Esen, I.; Özarpa, C.; Eltaher, M. A. Dynamics of perforated nanobeams subject to moving mass using the nonlocal strain gradient theory. *Applied Mathematical Modelling*, 2021, 96, pp. 215-235. https://doi.org/10.1016/j.apm.2021.03.008

[2] Almitani, K. H.; Abdelrahman, A. A.; Eltaher, M. A. Stability of perforated nanobeams incorporating surface energy effects. *Steel and Composite Structures*, 2020, 35 (4), pp. 555-566. https://doi.org/10.12989/scs.2020.35.4.555

[3] Abdelrahman, A. A.; Mohamed, N. A.; Eltaher, M. A. Static bending of perforated nanobeams including surface energy and microstructure effects. *Engineering with Computers*, 2022, 38, pp. 415-435. https://doi.org/10.1007/s00366-020-01149-x

[4] Esen, I.; Abdelrahman, A. A.; Eltaher, M. A. Dynamics analysis of Timoshenko perforated microbeams under moving loads. *Engineering with Computers*, 2022, 38, pp. 2413-2429. https://doi.org/10.1007/s00366-020-01212-7

[5] Eltaher, M. A.; Abdelrahman, A. A. Bending behavior of squared cutout nanobeams incorporating surface stress effects. *Steel and Composite Structures*, 2020, 36 (2), pp. 143-161. https://doi.org/10.12989/scs.2020.36.2.143

[6] Eltaher, M. A.; Mohamed, N. A. Vibration of nonlocal perforated nanobeams with general boundary conditions. *Smart Structures and Systems*, 2020, 25 (4), pp. 501-514. https://doi.org/10.12989/sss.2020.25.4.501

[7] Abdelrahman, A. A.; Eltaher, M. A. On bending and buckling responses of perforated nanobeams including surface energy for different beams theories. *Engineering with Computers*, 2022, 38, pp. 2385-2411. https://doi.org/10.1007/s00366-020-01211-8

[8] Eltaher, M. A. et al. Mechanical behaviors of piezoelectric nonlocal nanobeam with cutouts. *Smart Structures and Systems*, 2020, 25 (2), pp. 219-228. https://doi.org/10.12989/sss.2020.25.2.219

[9] Eltaher, M. A. et al. Mechanical analysis of cutout piezoelectric nonlocal nanobeam including surface energy effects. *Structural Engineering and Mechanics*, 2020, 76 (1), pp. 141-151. https://doi.org/10.12989/sem.2020.76.1.141

[10] Abdelrahman, A. A. et al. Free and forced analysis of perforated beams. *Steel and Composite Structures*, 2019, 31 (5), pp. 489-502. https://doi.org/10.12989/scs.2019.31.5.489

[11] Eltaher, M. A.; Abdraboh, A. M.; Almitani, K. H. Resonance frequencies of size dependent perforated nonlocal nanobeam. *Microsystem Technologies*, 2018, 24, pp. 3925-3937. https://doi.org/10.1007/s00542-018-3910-6

[12] Eltaher, M. A.; Kabeel, A. M.; Almitani, K. H.; Abdraboh, A. M. Static bending and buckling of perforated nonlocal size-dependent nanobeams. *Microsystem Technologies*, 2018, 24, pp. 4881-4893. https://doi.org/10.1007/s00542-018-3905-3

[13] Bourouina, H.; Yahiaoui, R.; Sahar, A.; Benamar, M. E. A. Analytical modeling for the determination of nonlocal resonance frequencies of perforated nanobeams subjected to temperature-induced loads. *Physica E: Low-dimensional Systems and Nanostructures*, 2016, 75, pp. 163-168. https://doi.org/10.1016/j.physe.2015.09.014

[14] Chakraverty, S.; Behera, L. *Static and dynamic problems of nanobeams and nanoplates*. World Scientific Publishing Co. Pte. Ltd., 2016. https://doi.org/10.1142/10137

[15] Luschi, L.; Pieri, F. A simple analytical model for the resonance frequency of perforated beams. *Procedia Engineering*, 2012, 47, pp. 1093-1096. https://doi.org/10.1016/j.proeng.2012.09.341

[16] Luschi, L.; Pieri, F. An analytical model for the determination of resonance frequencies of perforated beams. *Journal of Micromechanics and Microengineering*, 2014, 24 (5). https://doi.org/10.1088/0960-1317/24/5/055004

[17] Luschi, L.; Pieri, F. An analytical model for the resonance frequency of square perforated Lamé-mode resonators. *Sensors and Actuators B: Chemical*, 2016, 222, pp. 1233-1239. https://doi.org/10.1016/j.snb.2015.07.085

[18] Tauchert, T. R. *Energy Principles in Structural Mechanics*. New York, USA: McGraw-Hill Book Company Inc, 1974.

[19] Reddy J. N. Nonlocal nonlinear formulations for bending of classical and shear deformation theories of beams and plates. *International Journal of Engineering Science*, 2010, 48 (11), pp. 1507-1518. https://doi.org/10.1016/j.ijengsci.2010.09.020